

1 **Microbial strong organic ligand production is tightly coupled to iron in** 2 **hydrothermal plumes**

3
4 Colleen L. Hoffman^{1,2,3*†} and Patrick J. Monreal^{3,4*†}, Justine B. Albers⁵, Alastair J.M. Lough⁶, Alyson E.
5 Santoro⁵, Travis Mellett^{3,7}, Kristen N. Buck^{7,8}, Alessandro Tagliabue⁹, Maeve C. Lohan⁶, Joseph A.
6 Resing^{1,2,3}, Randelle M. Bundy³

7
8 ¹Joint Institute for the Study of Atmosphere and Ocean, University of Washington, 3737 Brooklyn
9 Avenue NE, Seattle, WA 98195, USA

10 ²Cooperative Institute for Climate, Ocean, and Ecosystem Studies, University of Washington,
11 3737 Brooklyn Avenue NE, Seattle, WA 98195, USA

12 ³School of Oceanography, University of Washington, 1501 NE Boat Street, Seattle, WA 98195,
13 USA

14 ⁴Earth Systems Program, Stanford University, 473 Via Ortega, Stanford, CA 94305,
15 USA

16 ⁵Department of Ecology, Evolution, and Marine Biology, University of California, Santa Barbara,
17 CA 93106, USA

18 ⁶Department of Ocean and Earth Sciences, National Oceanography Centre, University of
19 Southampton, European Way, Southampton SO14 3ZH, United Kingdom

20 ⁷College of Marine Science, University of South Florida, 140 7th Avenue South, St. Petersburg,
21 FL, 33701, USA

22 ⁸College of Earth, Oceans, and Atmospheric Sciences, Oregon State University, 2651 SW Orchard Ave,
23 Corvallis, OR, 97331, USA

24 ⁹Department of Earth, Ocean, and Ecological Sciences, University of Liverpool, 4 Brownlow
25 Street, Liverpool l69 3GP, United Kingdom

26
27 †These authors contributed equally and should be considered co-first authors

28 *Correspondence: ~~Colleen L. Hoffman and Patrick J. Monreal~~ Colleen L. Hoffman and Patrick J. Monreal

29
30 **Email:** clhoffma@gmail.com, pmonreal@uw.edu

31

32

33

34

35 **Abstract.** Hydrothermal vents have emerged as an important source of iron to seawater, yet only a subset of
36 ~~this~~ iron is soluble and persists long enough to ~~be available for surface biological uptake~~ ~~impact the deep~~
37 ~~ocean iron inventory~~. The longevity and solubility of iron in seawater is ~~in part~~ governed by strong organic
38 ligands, like siderophores, that are produced by ~~marine~~ microorganisms and are a part of the ocean's
39 dissolved ~~organic~~ iron-binding ligand pool. These ligands have been hypothesized to aid in the persistence
40 of dissolved iron in hydrothermal environments. To explore this hypothesis, we measured iron ~~and iron-~~
41 ~~binding, iron-binding~~ ligands ~~including, and~~ siderophores from 11 geochemically distinct sites along a 1,700
42 km section of the Mid-Atlantic Ridge. Siderophores were found in hydrothermal plumes at all sites, with
43 proximity to the vent playing an important role in dictating siderophore types and diversity. The notable
44 presence of amphiphilic siderophores may point to microbial utilization of siderophores to access particulate
45 hydrothermal iron, and the exchange of dissolved and particulate iron. The tight coupling between strong
46 ligands and dissolved iron within neutrally buoyant plumes across ~~six~~ distinct hydrothermal environments,
47 and the presence of dissolved siderophores with siderophore-producing microbial genera, suggests that
48 biological production of ~~siderophores-ligands~~ exerts a key control on hydrothermal dissolved iron
49 concentrations.

50 1. Introduction

51 Over the last few decades, observations and modelling efforts have increased our understanding about the
52 critical role organic ligands play in the cycling, transport, and utilization of trace metals (Tagliabue et al.,
53 2017; Buck et al., 2018; Bundy et al., 2018; Moore et al., 2021). ~~Iron (Fe) binding organic ligands in seawater~~
54 ~~have a wide range of sources, which are only just beginning to be understood.~~ ~~Recent~~ ~~but~~ observations
55 ~~suggest that microbial production of siderophores, humic-like substances and exopolysaccharides are some~~
56 ~~of the major contributors of marine organic ligands~~ (Hassler et al., 2017) ~~(Hassler et al. 2017), and linking~~
57 ~~microbial activity to impacts on Fe cycling. For example, in~~ ~~Microbial communities organic ligand~~
58 ~~production is thought to tightly control global~~ ~~can influence Fe inventories~~ ~~cycling in environments ranging~~
59 ~~from both~~ hydrothermal plumes (Cowen and Bruland, 1985; Cowen et al., 1990) ~~and to the open ocean~~
60 ~~(Lauderdale et al., 2020).~~ Strong ~~iron~~ Fe-binding organic ligands (L_1) are a heterogeneous mixture of
61 microbially produced compounds that are operationally classified based on their binding strength with ~~iron~~
62 (Fe) (defined as $\log K_{Fe, FeL}^{cond} > 12$). ~~They, and~~ are thermodynamically favored to complex and stabilize
63 external sources of Fe to prevent its scavenging and removal. ~~For~~ ~~As an~~ example, in high ~~dissolved and~~
64 ~~particulate~~-Fe estuarine systems, only the dissolved Fe (dFe) bound to the strongest Fe-binding ligands ~~is~~
65 ~~protected from scavenging and~~ remains in solution (Bundy et al., 2015; Buck et al., 2007) ~~and is accessible~~
66 ~~for downstream biological uptake.~~

67

68 Siderophores are the strongest known Fe-binding organic ligands. They are produced by bacteria and fungi
69 to facilitate Fe uptake and ~~solubilization of~~solubilize otherwise inaccessible phases in the marine
70 environment (Butler, 2005; Manck et al., 2022). They have primarily been considered ~~as~~an important
71 microbial strategy for Fe acquisition in the low ~~-~~Fe ($d\text{Fe} < 0.5 \text{ nM}$) surface ocean (Vraspir and Butler, 2009;
72 Butler, 2005). However, siderophore uptake and biosynthesis genes were observed in >70% of Fe-related
73 bacterial transcripts ~~in a hydrothermal environment at in~~ Guaymas Basin (Li et al., 2014), have been identified
74 in oxygen-deficient zones (Moore et al., 2021), and ~~is are~~ a common Fe acquisition strategy within terrestrial
75 and pathogenic ecosystems (Sandy and Butler, 2009), ~~all of which are environments wherever~~ Fe
76 ~~concentrations are~~is orders of magnitude higher than ~~surface~~ seawater.

77

78 ~~Although Previous studies have both looked at other additional~~ unknown strong Fe-binding ligands ~~besides~~
79 ~~siderophores have been observed~~ in hydrothermal plumes ~~and throughout the deep ocean~~ (Buck et al., 2018),
80 ~~as well as and throughout the deep ocean as well as and~~ siderophores ~~have also been observed~~ observed below
81 the euphotic zone (Bundy et al., 2018). ~~However,~~ no previous studies have ever directly ~~characterized~~
82 ~~measured~~ siderophores in hydrothermal systems. ~~Some form of A~~ ‘stabilizing agent’ (i.e. ligands) has been
83 proposed for the long-range transport of hydrothermal ~~d~~Fe into the ocean interior. The role of strong Fe-
84 binding ligands in hydrothermal dFe transport represents an important ~~gap~~ knowledge gap ~~with in~~ how
85 hydrothermal vents may impact the ocean dFe inventory (Resing et al., 2015). Here, for the first time, we
86 identified siderophores and siderophore-producing microbes in 11 geochemically distinct hydrothermal
87 environments along the slow-spreading (20-50 mm/yr) Mid-Atlantic Ridge (MAR), ~~including F~~four black
88 smokers (high temperature, high Fe), four off-axis sites, one diffuse vent (low temperature, low Fe), one
89 alkaline vent (pH 9-11, very low Fe), and one non-vent fracture zone ~~were investigated using both~~
90 ~~competitive ligand exchange-adsorptive cathodic stripping voltammetry and state-of-the-art liquid~~
91 ~~chromatography coupled to electrospray ionization mass spectroscopy (Boiteau et al., 2016) in a targeted~~
92 ~~approach to identify discrete components of the L₁ ligands and to search for known siderophores. Microbial~~
93 ~~community analysis was also compared at three sites~~ to understand whether microbial ligand production
94 impacts the supply of hydrothermal dFe to the ocean. Overall, our results show microbially-produced
95 siderophores were present in all sites, and that strong L₁ ligands ~~are were~~ tightly coupled to hydrothermal
96 dFe in the ~~neutrally-buoyant plumes in this~~ system. ~~Strong The presence of~~ organic ligands produced by
97 bacteria ~~in hydrothermal systems suggest that they thus~~ play an ~~key important~~ role in deep ocean Fe ~~delivery~~
98 ~~from hydrothermal systems~~ cycling.

99 **2. Results and Discussion**

100 **2.1 The role of iron-binding ligands in hydrothermal plumes**

101 ~~Strong organic Fe-binding ligands (defined here as ~~-or-~~L₁ ligands)~~ have been found to be important in
102 ~~neutrally-buoyant hydrothermal plumes (Tagliabue et al., 2017; Resing et al., 2015; Buck et al., 2018).~~ ~~But~~
103 ~~the relationship between organic ligands and dFe have never been investigated together systematically across~~

104 a wide variety of vents in the same study. In this work, the average binding strength and concentration of
105 organic Fe-binding ligands were quantified in 11 vent systems that spanned a wide range in dFe
106 concentrations (0.41-90 nM) and underlying vent geology. Over 99% of dFe in the neutrally buoyant plumes
107 were complexed by L₁ ligands and the ligands were almost always completely saturated with dFe, meaning
108 Fe-free 'excess' L₁ ligands capable of binding additional Fe were present in low concentrations (< 1 nM; **Fig.**
109 **S1**). As a result, dFe concentrations were tightly coupled to L₁ ligands in a nearly 1:1 ratio (**Fig. 1d**), similar
110 to previous studies in other neutrally buoyant plumes (**Fig. 1e**) (Lough et al., 2022; Buck et al., 2018, 2015).
111 The strong coupling between dFe and ligands was only observed at sites where L₁ ligands were detected.
112 Some sampling locations, such as in the buoyant plume or closer to the vent orifice, contained high
113 concentrations of weaker ligands ($\log K_{Fe, FeL}^{cond} < 12$, **Table S2**) with no correlation to dFe. This is consistent
114 with these environments likely being dominated by inorganic forms of Fe as hydrothermal fluids initially
115 mix with oxygenated seawater.

116
117 Our results indicate that L₁ ligands cap the dFe concentration in neutrally buoyant plumes. A similar control
118 on dFe concentrations by L₁ ligands has been previously observed in estuaries (Buck et al., 2007) and aerosol
119 solubility experiments (Fishwick et al., 2014). One possible explanation is that both the dFe and L₁ ligands
120 originate from the vent fluids themselves, yielding a tightly coupled hydrothermal endmember. However, the
121 concentration of L₁ ligands did not correlate with excess mantle Helium-3 (³He_{xs}, **Fig S2, Table S2**) (Lough
122 et al., 2022), a nearly conservative tracer of the mixing of hydrothermal fluids with seawater (Buck et al.,
123 2018), and our samples closer to the vent source were dominated by weaker organic ligands showing no
124 correlation to dFe. This suggests the L₁ ligands were not directly sourced from the vent fluids along with dFe.
125 Another explanation is the source of L₁ ligands observed in the neutrally-buoyant plume are either from
126 bacteria that produced them in surrounding deep ocean seawater that was then entrained, local production
127 from vent-biota and/or microbial mats, diffusion from microbial production in sediments, or *in-situ*
128 production by bacteria within the neutrally buoyant plume (Mellett et al., *submitted*).

130 2.2.12 Identity The presence of siderophores in hydrothermal systems

131 ~~Siderophores were measured in a subset of the samples (To further explore the source of the L₁ ligands we~~
132 ~~observed-coupled to dFe in the neutrally-buoyant plume samples, we measured siderophores in a subset of~~
133 ~~the samples. Marine organic ligand composition changes with environmental gradients (Boiteau et al., 2016;~~
134 ~~Gledhill and Buck, 2012), making the structure and functional groups of siderophores identified in and around~~
135 ~~hydrothermal samples of particular interest. Somewhat surprisingly, siderophores were found in all samples~~
136 ~~and we observed a large diversity of siderophores with high confidence using mass-to-charge ratio (*m/z*),~~
137 ~~MS/MS spectra, and specific chromatographic characteristics (Fig. 2a). Samples collected from o~~
138 ~~On-axis~~
139 ~~spreading centers contained the highest dFe concentrations (> 20 nM) and wider variety of siderophores than~~
samples from fracture zones, diffuse, and off-axis sites (dFe < 1 nM). The greatest number of distinct

140 siderophores were identified at Lucky Strike, Broken Spur, Rainbow, and TAG (Fig. 2). On average, 13
141 compounds were identified with high confidence per on-axis spreading center sample, compared with 5 per
142 diffuse/fracture zone sample, and 2.5 per off-axis sample (Fig. 2b, Fig. S4). Mixed-type siderophores —
143 containing different moieties that bind to Fe(III) — were common at all sites. Hydroxamates were identified
144 at and around spreading centers, yet none of these were detected with high confidence in samples from
145 diffuse/fracture zones (Fig. S4). Summed siderophore abundance in neutrally-buoyant plumes above
146 spreading centers was similarly more than twice that of samples from fracture zones or off-axis (Fig. 2c). ~~In~~
147 ~~this way~~ Thus, vent type and proximity played a role in the diversity and abundance of siderophore types
148 ~~produced~~ observed, likely related to the diversity of the microbial community and/or unique Fe acquisition
149 strategies across sites.

150
151 Siderophores are operationally part of the L₁ ligand pool based on their binding strength (Gledhill and Buck,
152 2012) and patterns in their distributions reflected those of the strong ligands. The peak areas of each putative
153 siderophore we identified were used as a proxy for concentrations (section 3.3), and these concentrations
154 significantly correlated with dFe, as observed with dFe and L₁ ligands (Fig. 2b). Siderophores were present
155 in concentrations similar to the surface ocean (Boiteau et al., 2016; Moore et al., 2021; Park et al., 2022;
156 Bundy et al., 2018), and comprised 0.01-0.4% of the total L₁ ligands (Table 1). This is likely a substantial
157 underestimate of siderophore contributions to the L₁ ligand pool due to analytical constraints in identifying
158 unknown siderophores. Recent work on siderophore biosynthesis pathways and advances in genome mining
159 suggest that known siderophores represent a small fraction of what is expected to be produced in nature
160 (Hider and Kong, 2010; Reitz et al., 2022). In addition, most siderophores are not commercially available to
161 use as standards, and individual siderophores have different ionization or extraction efficiencies. We
162 restricted our reporting to compounds only identified with very high confidence (Fig 2a, S3). The extraction
163 efficiency for the solid phase extraction technique is approximately 5-10% for bulk Fe-binding organics
164 (Bundy et al., 2018) and 40% for a siderophore standard (Waska et al., 2015). Employing both corrections
165 yields siderophore contributions to the total L₁ pool of 0.1-4% and 0.025-1%, respectively. We are inevitably
166 missing many naturally occurring unknown compounds. Regardless of the small percentage contribution to
167 total L₁ ligands, it is evident that microbially produced siderophores were ubiquitous across all vent sites and
168 had similar distributional patterns as L₁ ligands. The identification of siderophores — and their relationship
169 with dFe — provides compelling evidence that microbial production of ligands is responsible for at least
170 some portion of the tight coupling between L₁ and dFe in hydrothermal systems along the MAR.

171
172 The presence and diversity of siderophores identified in this system was surprising given the relatively high
173 Fe concentrations of hydrothermal environments, but some interesting patterns were observed. For example,
174 previous work has shown that ~~Low Fe surface waters in the ocean have higher concentrations of amphiphilic~~
175 ~~siderophores compared to high Fe coastal waters and terrestrial systems~~ (Boiteau et al., 2016), and
176 ~~amphiphilic siderophores are less common in terrestrial environments~~ (Hider and Kong, 2010). Amphiphilic

177 siderophores have long hydrocarbon tails that can be embedded into the lipid bilayer of the bacterial cell
178 membrane providing a mechanism to shuttle Fe into the cell and prevent diffusive loss (Martinez et al., 2003).
179 Amphiphilic siderophores accounted for ~~comprised~~ 57% of the siderophores in our samples (Fig. S5),
180 supporting the ubiquity of amphiphilic siderophores in ~~the~~ marine environments (Butler and Theisen, 2010).
181 ~~It was surprising they were so common, due to the elevated Fe concentrations observed relative to the Fe-~~
182 ~~poor surface ocean.~~ Amphiphilic siderophores were found in concentrations between 0.3-4.7 pM, with ~~the~~
183 ~~highest found at Rainbow (Fig. 2d, Table S5).~~ These concentrations were similar to those observed in the
184 upper ocean (Boiteau et al., 2016; Bundy et al., 2018; Boiteau et al., 2019). Marine bacteria produce suites
185 of amphiphilic siderophores as a way to adapt to the change in hydrophilicity in the surrounding environment
186 (Sandy and Butler, 2009; Homann et al., 2009). ~~Unlike in the surface ocean where amphiphilic siderophores~~
187 ~~are observed in Fe limited regions (Boiteau et al., 2016), a~~ Amphiphilic siderophores in plumes could be a
188 way for bacteria to access Fe as they are physically transported and cope with strong chemical gradients,
189 similar to the production of multiple siderophores in terrestrial and pathogenetic systems as a means to access
190 inorganic particulate Fe for cellular uptake and storage (Hider and Kong, 2010).

191 **2.21 The role of iron-binding ligands and siderophores in hydrothermal plumes**

192 Strong organic Fe binding ligands, or L₁ ligands, are important for stabilizing Fe in hydrothermal plumes
193 (Tagliabue et al., 2017; Resing et al., 2015; Buck et al., 2018). ~~The average binding strength and~~
194 ~~concentration of organic Fe binding ligands were quantified in multiple vent systems that spanned a wide~~
195 ~~range in dFe concentrations (0.41-90.3 nM) and underlying vent geology. Over 99% of dFe in the neutrally~~
196 ~~buoyant plumes were complexed by L₁ ligands and the ligands were almost always completely saturated with~~
197 ~~dFe, meaning Fe free ‘excess’ L₁ ligands capable of binding additional Fe were present in low concentrations~~
198 ~~(< 1 nM; Fig. S1). As a result, dFe concentrations were tightly coupled to L₁ ligands in a nearly 1:1 ratio~~
199 ~~(Fig. 1d), similar to previous studies in other neutrally buoyant plumes (Fig. 1c) (Lough et al., 2022; Buck~~
200 ~~et al., 2018, 2015). The strong coupling between dFe and ligands was only observed at sites where L₁ ligands~~
201 ~~were detected. Some sampling locations, such as in the buoyant plume, contained high concentrations of~~
202 ~~weaker ligands ($\log K_{Fe^2, FeL}^{cond} < 12$, Table S2) with no correlation to dFe.~~

203
204 Our results indicate that L₁ ligands uniquely set the dFe concentration in neutrally buoyant plumes. A similar
205 control of dFe concentrations by L₁ ligands has been previously observed in rivers (Buck et al., 2007) and
206 aerosol solubility experiments (Fishwick et al., 2014). One explanation is that both the dFe and L₁ ligands
207 originate from the vent fluids themselves, yielding a tightly coupled hydrothermal endmember. However, the
208 concentration of L₁ ligands did not correlate with excess mantle Helium-3 (³He_{xs}, Fig S2, Table S2) (Lough
209 et al., 2022), a nearly conservative tracer of the mixing of hydrothermal fluids with seawater (Buck et al.,
210 2018). These results suggest the L₁ ligands were not sourced from the vent fluids along with dFe. All known
211 sources of L₁ ligands are biologically produced. Therefore, the L₁ ligands observed here could be sourced
212 either from bacteria that produced them in the surrounding deep ocean seawater that was then entrained, local

213 production from vent biota and/or microbial mats, diffusion from microbial production in sediments, or *in-*
214 *situ* production by bacteria within the neutrally buoyant plume (Mellett et al., *submitted*).

215
216 Microbial organic ligand production is thought to tightly control global Fe inventories in both hydrothermal
217 plumes (Cowen and Bruland, 1985; Cowen et al., 1990) and the open ocean (Lauderdale et al., 2020).
218 Siderophores are operationally defined as L₁-ligands by their binding strength (Moore et al., 2021; Manek et
219 al., 2022) and have been proposed as important L₁-ligands in hydrothermal plumes (Li et al., 2014), though
220 they have never been directly measured. We used state of the art liquid chromatography coupled to
221 electrospray ionization mass spectroscopy (Boiteau et al., 2016) in a targeted approach to identify discrete
222 components of the L₁-ligands and to search for known siderophores. We observed a large diversity of
223 siderophores with high confidence in every vent site using mass to charge ratio (*m/z*), MS/MS spectra, and
224 specific chromatographic characteristics (Fig. 2a). Relative peak areas as a proxy for concentrations of
225 putative siderophores also significantly correlated with dFe, as observed with dFe and L₁-ligands (Fig. 2b).

226
227 Siderophores were present in concentrations similar to the surface ocean (Boiteau et al., 2016; Moore et al.,
228 2021; Park et al., 2022; Bundy et al., 2018), and comprised 0.01–0.4% of the total L₁-ligands (Table 1). This
229 is likely a significant substantial underestimate of siderophore contributions to the L₁-ligand pool due to
230 analytical constraints in identifying unknown siderophores. Recent work on siderophore biosynthesis
231 pathways and advances in genome mining suggest that, known siderophores represent a small fraction of
232 what is expected to be produced in nature (Hider and Kong, 2010). In addition, most siderophores are not
233 commercially available to use as standards, and individual siderophores have different ionization or
234 extraction efficiencies. We also restricted our reporting to compounds only identified with very high
235 confidence (Fig 2a, S3). The extraction efficiency for the solid phase extraction technique is around 5–10%
236 for bulk Fe-binding organics (Bundy et al., 2018) and 40% for a siderophore standard (Waska et al., 2015).
237 Employing both corrections yields siderophore contributions to the total L₁-pool of 0.1–4% and 0.025–1%,
238 respectively. Correcting for extraction efficiency of the identified siderophores yields contributions of 1–4%
239 of the L₁-pool. We are inevitably missing other many naturally occurring unknown compounds. Regardless
240 of the small percentage contribution to total L₁-ligands, it is evident that microbially produced siderophores
241 are ubiquitous across all vent sites.

242
243 The high diversity of siderophores across a huge range of hydrothermal vent systems reveals several
244 surprising aspects of Fe cycling. The biosynthesis of a siderophore is energy intensive and is regulated by Fe
245 concentration in the surrounding environment. Siderophore presence suggests that bacteria are producing
246 these compounds despite the overall higher Fe concentrations in the deep ocean and in hydrothermal plumes.
247 Consistent with siderophore utilization in terrestrial ecosystems, one hypothesis is that siderophore
248 production is beneficial to bacteria in the plumes for transforming Fe from otherwise inaccessible forms,
249 such as particulate nanopyrites or Fe oxyhydroxides. The identification of siderophores—and their

250 relationship with dFe—provides compelling evidence that microbial production of ligands is responsible
251 for some portion of the tight coupling between L_1 and dFe in hydrothermal systems along the MAR.
252

253 **2.2 Identity of siderophores in hydrothermal systems**

254 Marine ligand composition changes with environmental gradients (Boiteau et al., 2016), making the structure
255 and functional groups of siderophores identified in and around hydrothermal samples of particular interest.
256 Samples collected from on-axis spreading centers contained the highest dFe concentrations (> 20 nM) and
257 wider variety of siderophores than samples from fracture zones, diffuse, and off-axis sites ($dFe \leq 1$ nM). The
258 greatest number of distinct siderophores were identified at Lucky Strike, Broken Spur, Rainbow, and TAG
259 (Fig. 2). On average, 13 compounds were identified with high confidence per on-axis spreading center
260 sample, compared with 5 per diffuse/fracture zone sample, and 2.5 per off-axis sample (Fig. 2b, Fig. S4).
261 Mixed-type siderophores—containing different moieties that bind to Fe(III)—were common at all sites.
262 Hydroxamates were identified at and around spreading centers, yet none of these were detected with high
263 confidence in samples from diffuse/fracture zones (Fig. S4). Vent type and proximity played a role in the
264 diversity and abundance of siderophore types produced, likely related to the diversity of the microbial
265 community and/or unique Fe acquisition strategies across sites.
266

267 Low Fe surface waters in the ocean have higher concentrations of amphiphilic siderophores compared to high
268 Fe waters and terrestrial systems (Boiteau et al., 2016). Amphiphilic siderophores have long hydrocarbon
269 tails that can be embedded into the lipid bilayer of the bacterial cell membrane providing a mechanism to
270 shuttle Fe into the cell and prevent diffusive loss (Martinez et al., 2003). Amphiphilic siderophores accounted
271 for 57% of the siderophores in our samples (Fig. S5), supporting the ubiquity of amphiphilic siderophores in
272 the marine environment (Butler and Theisen, 2010). It was surprising they were so common, due to the
273 elevated Fe concentrations observed relative to the Fe-poor surface ocean. Amphiphilic siderophores were
274 found in concentrations between 0.3–4.7 pM, with highest found at Rainbow (Fig. 2d, Table S5). These
275 concentrations were similar to those observed in the upper ocean (Boiteau et al., 2016; Bundy et al., 2018;
276 Boiteau et al., 2019). Marine bacteria produce suites of amphiphilic siderophores as a way to adapt to the
277 change in hydrophilicity in the surrounding environment (Sandy and Butler, 2009; Homann et al., 2009).
278 Unlike in the surface ocean where amphiphilic siderophores are observed in Fe-limited regions (Boiteau et
279 al., 2016), amphiphilic siderophores in plumes could be a way for bacteria to access Fe as they are physically
280 transported and cope with strong chemical gradients, similar to the production of multiple siderophores in
281 terrestrial and pathogenetic systems as a means to access inorganic particulate Fe for cellular uptake and
282 storage (Hider and Kong, 2010).
283

284 2.3 Microbial sources of siderophores in hydrothermal plumes

285 The high diversity of siderophores across a huge range of hydrothermal vent systems revealed several
286 surprising aspects of Fe cycling. The biosynthesis of a siderophore is energy-intensive and is regulated by Fe
287 concentration in the surrounding environment (Rizzi et al., 2019) ~~(Rizzi et al., 2019)~~. Siderophore presence
288 suggests that bacteria are producing these compounds despite the overall higher Fe concentrations in the deep
289 ocean and within hydrothermal plumes. Consistent with siderophore utilization in terrestrial ecosystems
290 (Hider and Kong, 2010; Sandy and Butler, 2009), one hypothesis is that siderophore production is beneficial
291 to bacteria in the plumes for transforming Fe from otherwise inaccessible forms, such as particulate
292 nanopyrites or Fe oxyhydroxides. To explore mMicrobial production of siderophores, ~~is a strategy for~~
293 ~~organisms to adapt or compete with others for Fe (Sandy and Butler, 2009)~~. We examined microbial
294 community composition around Rainbow (St. 11, 17) and Lucky Strike (St. 7; **Table 1, Table S1**) using 16S
295 rRNA gene-based amplicon sequencing to detect bacteria with the metabolic potential to synthesize
296 siderophores (**Fig. 3, S11**), where the presence of taxa encoding siderophore biosynthetic gene clusters
297 indicates whether the microbial community is genetically capable of producing the compounds we observed.
298 Bacterial genera containing known siderophore-producers were found at all three MAR sites examined, and
299 putative siderophore-producers represented 3-20% of the relative abundance of ~~each the~~ community (**Fig. 3**).
300 Putative siderophore-producers were more abundant in the 3 μm (particle-attached) size fraction than in the
301 0.2 μm (free-living) fraction, suggesting siderophore production is more common in particle-associated
302 bacteria in hydrothermal environments.

303

304 We found microbial genera in our samples that can produce a subset of the siderophores identified here,
305 including ferrioxamines, vibrioferrin, and acinetoferrin (Butler, 2005; Vraspir and Butler, 2009; Moore et al.,
306 2021; Bundy et al., 2018; Boiteau et al., 2016). Genera with the genetic potential to produce ferrioxamines
307 were present at all three sites, while those known to produce vibrioferrin were present at Lucky Strike and
308 Rainbow, and those producing acinetoferrin were also present at Rainbow (**Table S1, S6**). Mycobactins were
309 detected with high confidence in every sample of this study, and genes encoding mycobactin have been
310 detected in a cultured organism from a hydrothermal system (Gu et al., 2019), but no mycobactin producers
311 were identified in this study. We detected woodybactin D with high confidence in 5 out of 11 sites. Although
312 these biosynthetic genes were not identified in any of the genera observed, woodybactin D is a carboxylate
313 siderophore isolated from *Shewanella* (Carmichael et al., 2019), and groups of deep-sea *Shewanella* (Kato
314 and Nogi, 2001) were found in the dataset (**Fig. S11**). The biosynthesis genes for many of the siderophores
315 identified are unknown. Thus, finding genera capable of producing only a subset of the siderophores
316 characterized is not surprising. The observation that a significant portion of the *in-situ* microbial community
317 is capable of synthesizing siderophores (**Fig 3**) suggests that siderophore production is more widespread in
318 the ~~marine environment and~~ deep ocean than previously believed.

319

320 2.4 The impact of strong ligands and siderophores on dissolved iron in neutrally-buoyant plumes

321 ~~Although siderophores are often assumed to be associated primarily with low Fe conditions, e~~Evidence that
322 siderophores are ubiquitous in the marine environment — including higher Fe ~~ones environments~~ — has
323 been increasing (Park et al., 2023). The higher dFe associated with hydrothermal plumes may still not be
324 high enough to suppress siderophore production due to the ~~elevated~~ Fe requirements of ~~heterotrophic~~ bacteria
325 (Tortell et al., 1996). It is also likely that in hydrothermal plumes not all of the Fe is bio-accessible. ~~For~~
326 ~~example, s~~Soil microbes secrete siderophores to solubilize particulate Fe (Crowley et al., 1991) ~~and, s~~Similar
327 processes could be occurring in hydrothermal plumes, where Fe mineral phases ~~associated with organic~~
328 ~~compounds~~ are common ~~and have been shown to be associated with organics~~ (Hoffman et al., 2020; Toner
329 et al., 2009). ~~Although our measurements suggest that dFe in the neutrally-buoyant plume is dominated by~~
330 ~~organic complexation, the L₁ measurements alone cannot distinguish between purely organic phases or a~~
331 ~~mixture of inorganic and organic ligands in complex aggregations or small colloids. Given the evidence from~~
332 ~~particulate Fe studies in neutrally-buoyant plumes (Hoffman et al. 2020), it is highly likely that some portion~~
333 ~~of what is detected in the L₁ pool is a mixture of organic and inorganic Fe in small colloids which are~~
334 ~~operationally in the dFe pool (Fitzsimmons et al., 2017). It is also~~ telling that most siderophore-producing
335 genera were found to be particle-associated (**Fig. 3**), providing additional evidence that siderophores might
336 be produced to solubilize particulate Fe ~~or access other colloidal phases~~. Further work that assesses why
337 bacteria are producing siderophores in neutrally buoyant plumes will be important for understanding
338 ~~microbial metabolism in these systems, and the impact of siderophore production on Fe dispersal.~~

339
340 ~~Organic Fe-binding ligands have been implicated in playing a critical role in the preservation and transport~~
341 ~~of hydrothermal dFe into the ocean interior (Hoffman et al., 2018; Resing et al., 2015; Fitzsimmons et al.,~~
342 ~~2017; Toner et al., 2009; Bennett et al., 2011, 2008; Buck et al., 2018; Sander and Koschinsky, 2011). In this~~
343 ~~work, L₁ ligands were tightly coupled to dFe in neutrally buoyant plumes along the MAR and the presence~~
344 ~~of siderophores in these samples provided evidence for the first time, that at least some of these ligands are~~
345 ~~microbially produced. How~~the role of these complexes ~~in~~may ~~facilitate~~ing the exchange of Fe between
346 dissolved and particulate phases (Fitzsimmons et al., 2017), and ~~how whether Fe-siderophores~~ ~~complexes~~
347 ~~are present may be stabilizing dFe in hydrothermal plumes.~~

348
349 ~~Organic Fe binding ligands have been implicated in playing a critical role in the preservation and transport~~
350 ~~of hydrothermal Fe into the ocean interior (Hoffman et al., 2018; Resing et al., 2015; Fitzsimmons et al.,~~
351 ~~2017; Toner et al., 2009; Bennett et al., 2011, 2008; Buck et al., 2018; Sander and Koschinsky, 2011). In this~~
352 ~~work, L₁ ligands were tightly coupled to dFe in neutrally buoyant hydrothermal plumes along the MAR and~~
353 ~~found to be microbially produced. For the first time, specific siderophores were identified and demonstrated~~
354 ~~a bacterial source of L₁ ligands being produced in response to external hydrothermal Fe inputs. Most of the~~
355 ~~bacteria putatively capable of synthesizing siderophores were particle associated. This adds to a growing~~
356 ~~body of evidence that bacteria are using L₁ ligands or siderophores to access particulate Fe pools, which is a~~
357 ~~key mechanism for controlling dFe in neutrally buoyant plumes. Exploring whether the Fe organic ligand~~

358 ~~production is tightly coupled~~ across additional hydrothermal vent systems will aid in constraining the
359 biogeochemical importance of microbial feedbacks in impacting the hydrothermal dFe supply to the deep
360 ocean.

362 **3. Appendix: Materials and Methods**

363 **3.1 Sampling and cruise transect**

364 Samples were collected as part of the 2017-2018 U.K. GEOTRACES GA13 section cruise along the Mid-
365 Atlantic Ridge. Water samples from 11 venting and near venting locations were collected using a Seabird
366 911 conductivity, temperature, and depth (CTD) titanium rosette using conducting Kevlar wire with an
367 oxidation-reduction potential (ORP) sensor to detect plumes. Teflon coated OTE (Ocean Test Equipment)
368 bottles were pressurized to approximately 7 psi with 0.2 μm filtered air using an oil free compressor. A
369 Sartobran 300 (Sartorius) filter capsule (0.2 μm) was used to collect filtered seawater samples into clean 250
370 mL LDPE sample bottles. Bottles and caps were rinsed 3 times with the filtered sample before being filled.
371 Samples were stored frozen at -20°C for Fe-organic ligand characterization by voltammetry and mass
372 spectrometry.

373 **3.2 Fe-binding ligand concentration and binding strengths Competitive Ligand Exchange-Adsorptive** 374 **Cathodic Stripping Voltammetry**

375 Fe-binding ligand concentrations and binding strengths (defined as conditional binding constants, $\log K_{\text{Fe}, \text{FeL}}^{\text{cond}}$
376 > 12) were determined by competitive ligand exchange-adsorptive cathodic stripping voltammetry (CLE-
377 ACSV) with a BASi controlled growth mercury electrode (CGME) with an Ag/AgCl⁻ reference electrode
378 and platinum auxiliary electrode (Bioanalytical Systems Incorporated). Using previously established
379 methods (Buck et al., 2015, 2018; Bundy et al., 2018; Abualhaija and van den Berg, 2014; Hawkes et al.,
380 2013b), 40 frozen filtrate ($<0.2 \mu\text{m}$) samples with dFe concentrations between 0.41-11.67 nM (**Table S1-**
381 **S2**) were thawed in a 4°C fridge prior to analysis. A 15-point titration curve was analyzed for each sample.
382 Briefly, within each titration, every point sequentially received 10 mL of sample, 7.5 ~~m~~ μM of borate-
383 ammonium buffer, 10 μM salicylaloxime (SA) added ligand, and a dFe addition. Data was collected using
384 the *Epsilon Eclipse Electrochemical Analyzer* (v.213) with a deposition time of 120 seconds and analyzed
385 using *ElectroChemical Data Software* (v2001-2014) and *ProMCC* (v2008-2018) to determine peak areas and
386 Fe-binding ligand parameters, respectively. All results were confirmed to fall within the analytical window
387 of the method by comparing the side reaction coefficient of the added ligand α_{SA} to the side reaction
388 coefficient of the natural ligands detected (α_{L}). If the α_{L} was within an order of magnitude of α_{SA} then the
389 results were deemed to fall within the analytical window.

390 **3.3 Reverse Titration-CLE-ACSV**

391 Reverse titration-CLE-ACSV (RT-CLE-ACSV) (Hawkes et al., 2013a) was completed on 10 samples from
392 Broken Spur, and TAG hydrothermal vent fields with dFe concentrations between 19.01-90.25 nM (**Table**
393 **S1-S2**). Briefly, a 10-point titration curve was analyzed for each sample with each titration point consisting
394 of 10 mL of sample buffered with 7.5 ~~μ~~mM boric acid and the competitive ligand 1-nitroso-2-naphthol (NN)
395 additions. All samples were analyzed on a BASi Controlled Growth Mercury Electrode (CGME) with the
396 *Epsilon Eclipse Electrochemical Analyzer* (v.213) and deposition time of 120 seconds. For each sample,
397 competitive ligand NN additions were 0.5, 1, 2, 3, 4, 6, 9, 15, 20, and 40 μM. Samples were equilibrated
398 overnight and purged with N₂ (99.99%) for 5 minutes before analysis. At the end of each titration, three Fe
399 additions (3-15 nM) were added to the final titration point to get the total concentration of Fe in equilibrium
400 with ligands. Data was analyzed using *ElectroChemical Data Software* (v2001-2014) to acquire peak areas
401 and a package in R using the model parameters of $\beta_{\text{FeNN}_3} = 5.12 \times 10^{16}$, $\chi_{\text{min}} = 0.8$, $\chi_{\text{max}} = 0.9$, and $c_{\text{high}} =$
402 0.75 to determine the Fe-binding ligand parameters (Hawkes et al., 2013a). These parameters were chosen
403 based on the recommendations for undersaturated samples and titrations curves where ip_{max} was not reached
404 (Hawkes et al., 2013a). All other parameters within the model we kept at the default values.

405 **3.4 ~~Fe-binding organic ligand~~Siderophore quantification and characterization**

406 In addition to ~~determining the total concentrations of strong (L_1)~~measuring Fe-binding ligands by
407 voltammetry (~~L_1~~), we also identified and quantified siderophores ~~that contributed to the L_1 ligand pool~~.
408 Between 0.65-1.5 L of 0.2 μm filtered seawater pooled from ligand samples at each site (described above)
409 was pumped slowly (15-20 mL min⁻¹) onto a polystyrene-divinylbenzene (Bond Elut ENV) solid phase
410 extraction (SPE) column (Bundy et al., 2018; Boiteau et al., 2016). SPE columns were rinsed with MilliQ
411 and stored at -20°C until analysis. For the analytical measurements, samples were thawed in the dark, eluted
412 in 12 mL of distilled methanol, and dried down to between 0.2-0.5 mL of sample eluent (**Table S1**). Aliquots
413 were analyzed by reverse-phase liquid chromatography (LC) on a trace metal clean bio-inert LC (Thermo
414 Dionex 3000 NCS). The LC was interfaced with an electrospray ionization-mass spectrometer (ESI-MS;
415 Thermo Q-Exactive HF) to identify and quantify the compounds based on accurate mass (MS¹) and the
416 fragmentation (MS²) data (Bundy et al., 2018; Boiteau et al., 2016). MSconvert (Proteowizard) was used to
417 convert MS data to an open source mzxML format, and two stages of data processing were conducted using
418 modified versions of previously reported R scripts (Bundy et al., 2018; Boiteau et al., 2016). In the first stage,
419 mzxML files were read into R using new package “RaMS” (Kumler and Ingalls, 2022) ~~{Formatting~~
420 ~~Citation}~~(~~Kulmer and Ingalls, 2022~~), and extracted ion chromatograms (EICs) were generated for each
421 targeted m/z of interest from an in-house database of siderophores. The m/z targets were the ionized apo,
422 ⁵⁴Fe-bound, and ⁵⁶Fe-bound version of each siderophore, with a tolerance of 7.5 ppm. Putative siderophore
423 candidates were filtered through a series of hard thresholds, such that MS¹ spectra were quality controlled to
424 contain a minimum of 25 datapoints and the maximum intensity of each EIC was greater than 1e4 counts.
425 Spectra meeting these criteria and containing either ⁵⁴Fe-bound and ⁵⁶Fe-bound m/z peaks within 30 seconds

426 of each other or an apo peak were displayed for the user to further inspect peak quality and make the final
427 decision of whether to move on to stage two of processing with a given siderophore candidate.

428

429 Stage two of processing extracted MS² spectra of the apo and Fe-bound forms of candidate siderophores to
430 compare with the predicted MS² generated by *in silico* fragmenter MetFrag (Ruttkies et al., 2016). The *in*
431 *silico* fragmenter feature was run with a tolerance of 10 ppm on “[M+H]⁺” and “[M+Na]⁺” modes. A
432 confidence level of 1-4, from highest to lowest confidence, was then assigned to putative siderophores based
433 on the following criteria: (1) peaks were present in MS¹ and MS² spectra, and at least one of the three most-
434 intense MS² fragments matched *in silico* fragmentation, (2) peaks were present in MS¹ and MS² spectra, and
435 smaller-intensity fragments matched *in silico* fragmentation, (3) peaks were present in MS¹ and MS² spectra,
436 but little to no fragments matched *in silico* fragmentation, and (4) nicely shaped peaks were identified in MS¹
437 spectra but no MS² spectra was collected (outlined in **Table S4**; example spectra in **Fig. S6-S9**). The
438 confidence levels were modelled after reporting standards for metabolite identification (Sumner et al., 2007).
439 MetFrag pulls chemical structures from publicly-available databases like PubChem or COCONUT (Sorokina
440 et al., 2021), which contain most, but not all variations of siderophores. As such, Fe-bound candidates were
441 usually run against the apo form available in the database, and for siderophores with similar structures but
442 variations in fatty chain length or double bond placement, sometimes only one parent structure was available.

443

444 A 5-point standard curve with known concentrations of siderophore ferrioxamine E was used for
445 quantification of putative siderophores, with a limit of detection of 0.257 nM in the eluent (**Fig. S10**), or
446 0.07-0.21 pM in the sample depending on sample-to-eluent volume ratio at each site (**Table S1**). MS¹ peaks
447 were integrated for all putatively identified siderophores and peak areas were converted to concentration
448 using the standard curve and the concentration factor of sample volume to eluent volume (**Fig. S10**).
449 Commercial standards are not available for most siderophores, and different compounds have distinct
450 ionization efficiencies in ESI-MS. Thus, the siderophore concentrations reported here are estimates of
451 siderophore concentrations in these environments based on ferrioxamine E, [chosen for its commercial](#)
452 [availability and use in prior studies \(e.g., \(Boiteau et al., 2016\)Boiteau et al., 2016\).](#) -Additionally, 1 mM of
453 cyanocobalamin was added as an internal standard to each sample aliquot to address any changes in
454 sensitivity during LC-ESI-MS runs. All putative siderophores that were identified with peak areas less than
455 the detection limit were discarded, and all remaining putative compounds with at least confidence levels 1
456 and 2 at one site were included in the manuscript and are referred to as siderophores throughout. Siderophore
457 identifications remain putative due to inherent uncertainty with assignments by mass, but the confidence
458 levels were designed such that high confidence candidates contain siderophore-like moieties in their
459 fragments. Limited sample volumes prevented analysis via LC-ICP-MS like previous studies, which, in
460 addition to greater availability of commercial standards [and more analytical comparisons between](#)
461 [ferrioxamine E with other siderophore types](#), would allow definitive ~~identification~~ [characterization](#) in future
462 [workstudies](#). Confidence level 3 and 4 putative siderophores are only included in the Supplementary

463 Information (**Table S5**). In a final step of quality control, EICs for ¹³C isotopologues of candidates were
464 inspected to verify matching peak structure.

465 **3.5 Microbial community analysis**

466 Microbial community composition was assessed in neutrally buoyant plumes and near venting sites at three
467 sites: Lucky Strike (Station 7; 1670 m), 10 km S of Rainbow (Station 17; 2000 m), and 200 km E of Rainbow
468 (Station 11; 600 m, 1600 m and 2250 m). A range of 1- 2 L of seawater were filtered by pressure filtration
469 through sequential 25 mm membrane filters housed in polypropylene filter holders (Whatman SwinLok, GE
470 Healthcare, Pittsburgh, Pennsylvania) using a peristaltic pump and silicone tubing. Samples first passed
471 through a 3 µm pore-size polyester membrane filter (Sterlitech, Auburn, Washington) then onto a 0.2 µm
472 pore-size polyethersulfone membrane filter (Supor-200, Pall Corporation, Port Washington, New York).
473 Pump tubing was acid washed with 10% hydrochloric acid and flushed with ultrapure water between each
474 sample. The filters were flash frozen in liquid nitrogen in 2 mL gasketed bead beating tubes (Fisher Scientific)
475 at sea.

476

477 Nucleic acids (DNA) were extracted as described previously (Santoro et al., 2010), with slight modifications.
478 Briefly, cells on the filters were lysed directly in the bead beating tubes with sucrose-ethylene diamine
479 tetraacetic acid (EDTA) lysis buffer (0.75 M sucrose, 20 mM EDTA, 400 mM NaCl, 50 mM Tris) and 1%
480 sodium dodecyl sulfate. Tubes were then agitated in a bead beating machine (Biospec Products) for 1 min,
481 and subsequently heated for 2 min. at 99°C in a heat block. Proteinase K (New England Biolabs) was added
482 to a final concentration of 0.5 mg/mL. Filters were incubated at 55°C for approximately 4 h and the resulting
483 lysates were purified with the DNeasy kit (Qiagen) using a slightly modified protocol (Santoro et al., 2010).
484 The purified nucleic acids were eluted in 200 µL of DNase, RNase-free water, and quantified using a
485 fluorometer (Qubit and Quanti-T HS reagent, Invitrogen Molecular Probes).

486

487 The 16S rRNA gene was amplified in all samples using V4 primers (Apprill et al., 2015; Parada et al., 2016)
488 (515F-Y and 806RB) following a previously established protocol (Stephens et al., 2020). Amplicons were
489 sequenced using a paired-end 250bp run on an Illumina MiSeq 500 and demultiplexed by the UC Davis
490 Genome Center. The resulting 16S rRNA amplicon sequences were filtered and trimmed using the DADA2
491 pipeline in R (Callahan et al., 2016). Taxonomic assignments were made with version 138.1 of the SILVA
492 SSU database (Quast et al., 2013) (silva_nr99_v138.1_wSpecies_train_set.fa.gz ;
493 doi:10.5281/zenodo.4587955; accessed March 2022). Chloroplast and mitochondrial sequences were filtered
494 out of the dataset using the 'phyloseq' R package (v 1.38.0), after which samples had read depths ranging
495 from 9375 – 65486 reads (average 28425 ± 20014 reads) and represented 1010 unique amplicon sequence
496 variants (ASVs). Read counts were transformed from absolute to relative abundance and taxa were
497 aggregated to the Family level. The ten most abundant families present in each sample were visualized using
498 the 'ggplot2' package (v. 3.3.5).

499

500 In order to assess the potential of the observed prokaryotic taxa to produce siderophores, we downloaded all
501 siderophore biosynthetic gene clusters (BGCs) in the antimash secondary metabolite database ($n = 7909$)
502 and used text-string matching to compare genera containing these BGCs to the genera found in our 16S rRNA
503 gene dataset (Blin et al., 2021). We cross-referenced the nomenclature of antimash-predicted siderophores
504 with that of the siderophores identified by LC-ESI-MS in this study, accounting for minor differences in
505 naming convention between the two databases, to determine if microbial community members present at
506 each site were predicted to make any of the siderophores that were measured at that site. Station 38 and
507 Station 12 were the closest sites with siderophore measurements for comparison against the taxonomic
508 samples taken at 200 km E of Rainbow and 10 km S of Rainbow, respectively. Samples for microbial
509 taxonomy and siderophore identity were taken from the same location at Lucky Strike and thus directly
510 compared.

511

512 **Data Availability**

513 The CSV data reported in this study has been deposited at Zenodo under the DOI:
514 <http://doi.org/10.5281/zenodo.7325154>. The LC-ES-MS data has been deposited on Massive under the DOI:
515 <http://doi.org/doi.10.25345/C5V97ZW7N>. Microbial 16S rRNA data have been deposited on GenBank under
516 the accession number BioProject #PRJNA865382. All data is freely available on each of these data
517 repositories.

518

519

520 **Acknowledgments**

521 We acknowledge the captain and crew of the R/V *James Cook*, Chief Scientist Alessandro Tagliabue, and
522 Noah Gluschankoff for supporting this work. This study was a part of the FeRidge project (GEOTRACES
523 section GA13) which was supported by the Natural Environment Research Council funding (NERC United
524 Kingdom Grants NE/N010396/1 to MCL and NE/N009525/1 to AT). The International GEOTRACES
525 Programme is possible in part thanks to the support from the U.S. National Science Foundation (Grant OCE-
526 1840868) to the Scientific Committee on Oceanic Research (SCOR). CLH was funded by JISAO/CICOES
527 postdoctoral fellowship. PJM was funded through the NOAA Hollings Scholar summer program. JR was
528 funded by NOAA Ocean Exploration and Research, NOAA Earth-Ocean Interactions programs at NOAA-
529 Pacific Marine Environmental Labs, and JISAO/CICOES. Part of this work was carried out in the University
530 of Washington TraceLab, which receives support from the M.J. Murdock Charitable Trust in conjunction
531 with the University of Washington College of Environment, and the Pacific Marine Environmental Labs at
532 the National Oceanic and Atmospheric Administration. Parts of this work was also carried out in Dr. Anitra
533 Ingalls laboratory with the help of Laura Truxal and Dr. Jiwoon Park at the University of Washington-School
534 of Oceanography.

535

536 **Author Contributions:** Manuscript preparation, sample/data processing, CSV analysis, and interpretation
537 (~~C.L.H.~~), ~~manuscript preparation~~, LC-ESI-MS data analysis and interpretation (C.L.H. and P.J.M.), microbial
538 analysis and interpretation (J.B.A. and A.E.S.), dissolved iron and derived excess $^3\text{He}_{\text{xs}}$ measurements,
539 sample collection (A.J.M. L. and M.C.L.), microbial data collection and ligand data interpretation (T.M. and
540 K.N.B.), and project design and planning, data interpretation, and mentoring (A.T., M.C.L., J.A.R., and
541 R.M.B.). All authors were involved in editing and revision of the manuscript.

542

543 **Competing Interest Statement:** The authors declare no competing interests.

544

545 **References**

546 Abualhaija, M. M. and van den Berg, C. M. G. G.: Chemical speciation of iron in seawater using catalytic
547 cathodic stripping voltammetry with ligand competition against salicylaldoxime, *Mar. Chem.*, 164, 60–74,
548 <https://doi.org/10.1016/j.marchem.2014.06.005>, 2014.

549 Apprill, A., McNally, S., Parsons, R., and Weber, L.: Minor revision to V4 region SSU rRNA 806R gene
550 primer greatly increases detection of SAR11 bacterioplankton, *Aquat. Microb. Ecol.*, 75, 129–137,
551 <https://doi.org/10.3354/ame01753>, 2015.

552 Bazylev, B. A.: Allochemical Metamorphism of Mantle Peridotites in the Hayes Fracture Zone of the North
553 Atlantic, *Petrology*, 5, 362–379, 1997.

554 Beaulieu, S. E. and Szafranski, K. M.: InterRidge Global Database of Active Submarine Hydrothermal Vent
555 Fields Version 3.4, <https://doi.org/10.1594/PANGAEA.917894>, 2020.

556 Bennett, S. a., Achterberg, E. P., Connelly, D. P., Statham, P. J., Fones, G. R., and German, C. R.: The
557 distribution and stabilisation of dissolved Fe in deep-sea hydrothermal plumes, *Earth Planet. Sci. Lett.*, 270,
558 157–167, <https://doi.org/10.1016/j.epsl.2008.01.048>, 2008.

559 Bennett, S. a., Hansman, R. L., Sessions, A. L., Nakamura, K. ichi, and Edwards, K. J.: Tracing iron-fueled
560 microbial carbon production within the hydrothermal plume at the Loihi seamount, *Geochim. Cosmochim.*
561 *Acta*, 75, 5526–5539, <https://doi.org/10.1016/j.gca.2011.06.039>, 2011.

562 Blin, K., Shaw, S., Kautsar, S. A., Medema, M. H., and Weber, T.: The antiSMASH database version 3:
563 Increased taxonomic coverage and new query features for modular enzymes, *Nucleic Acids Res.*, 49, D639–
564 D643, <https://doi.org/10.1093/nar/gkaa978>, 2021.

565 Boiteau, R. M., Mende, D. R., Hawco, N. J., McIlvin, M. R., Fitzsimmons, J. N., Saito, M. A., Sedwick, P.
566 N., DeLong, E. F., and Repeta, D. J.: Siderophore-based microbial adaptations to iron scarcity across the
567 eastern Pacific Ocean, *Proc. Natl. Acad. Sci.*, 113, 14237–14242, <https://doi.org/10.1073/pnas.1608594113>,
568 2016.

569 Boiteau, R. M., Till, C. P., Coale, T. H., Fitzsimmons, J. N., Bruland, K. W., and Repeta, D. J.: Patterns of
570 iron and siderophore distributions across the California Current System, *Limnol. Oceanogr.*, 64, 376–389,
571 <https://doi.org/10.1002/lno.11046>, 2019.

572 Buck, K. N., Lohan, M. C., Berger, C. J. M., and Bruland, K. W.: Dissolved iron speciation in two distinct
573 river plumes and an estuary: Implications for riverine iron supply, *Limnol. Oceanogr.*, 52, 843–855,
574 <https://doi.org/10.4319/lo.2007.52.2.0843>, 2007.

575 Buck, K. N., Sohst, B., and Sedwick, P. N.: The organic complexation of dissolved iron along the U.S.

576 GEOTRACES (GA03) North Atlantic Section, Deep. Res. Part II Top. Stud. Oceanogr., 116, 152–165,
577 <https://doi.org/10.1016/j.dsr2.2014.11.016>, 2015.

578 Buck, K. N., Sedwick, P. N., Sohst, B., and Carlson, C. A.: Organic complexation of iron in the eastern
579 tropical South Pacific: Results from US GEOTRACES Eastern Pacific Zonal Transect (GEOTRACES cruise
580 GP16), *Mar. Chem.*, 201, 229–241, <https://doi.org/10.1016/j.marchem.2017.11.007>, 2018.

581 Bundy, R. M., Abdulla, H. A. N., Hatcher, P. G., Biller, D. V., Buck, K. N., and Barbeau, K. A.: Iron-binding
582 ligands and humic substances in the San Francisco Bay estuary and estuarine-influenced shelf regions of
583 coastal California, *Mar. Chem.*, 173, 183–194, <https://doi.org/10.1016/j.marchem.2014.11.005>, 2015.

584 Bundy, R. M., Boiteau, R. M., McLean, C., Turk-Kubo, K. A., McIlvin, M. R., Saito, M. A., Mooy, B. A.
585 Van, and Repeta, D. J.: Distinct Siderophores Contribute to Iron Cycling in the Mesopelagic at Station
586 ALOHA, *Front. Mar. Sci.*, 1–15, <https://doi.org/10.3389/fmars.2018.00061>, 2018.

587 Butler, A.: Marine siderophores and microbial iron mobilization., *Biometals*, 18, 369–374,
588 <https://doi.org/10.1007/s10534-005-3711-0>, 2005.

589 Butler, A. and Theisen, R. M.: Iron(III)-siderophore coordination chemistry: Reactivity of marine
590 siderophores., *Coord. Chem. Rev.*, 254, 288–296, <https://doi.org/10.1016/j.ccr.2009.09.010>, 2010.

591 Callahan, B. J., McMurdie, P. J., Rosen, M. J., Han, A. W., Johnson, A. J. A., and Holmes, S. P.: DADA2:
592 High-resolution sample inference from Illumina amplicon data, *Nat. Methods*, 13, 581–583,
593 <https://doi.org/10.1038/nmeth.3869>, 2016.

594 Carmichael, J. R., Zhou, H., and Butler, A.: A suite of asymmetric citrate siderophores isolated from a marine
595 *Shewanella* species, *J. Inorg. Biochem.*, 198, 1–6, <https://doi.org/10.1016/j.jinorgbio.2019.110736>, 2019.

596 Cowen, J. P. and Bruland, K. W.: Metal deposits associated with bacteria: implications for Fe and Mn marine
597 biogeochemistry, *Deep Sea Res. Part A. Oceanogr. Res. Pap.*, 32, 253–272, [https://doi.org/10.1016/0198-0149\(85\)90078-0](https://doi.org/10.1016/0198-0149(85)90078-0), 1985.

599 Cowen, J. P., Massoth, G. J., and Feely, R. A.: Scavenging rates of dissolved manganese in a hydrothermal
600 vent plume, *Deep Sea Res. Part A. Oceanogr. Res. Pap.*, 37, 1619–1637, [https://doi.org/10.1016/0198-0149\(90\)90065-4](https://doi.org/10.1016/0198-0149(90)90065-4), 1990.

602 Crowley, D. E., Wang, Y. C., Reid, C. P. P., and Szaniszlo, P. J.: Mechanisms of iron acquisition from
603 siderophores by microorganisms and plants, *Plant Soil*, 130, 179–198, 1991.

604 Fishwick, M. P., Sedwick, P. N., Lohan, M. C., Worsfold, P. J., Buck, K. N., Church, T. M., and Ussher, S.
605 J.: The impact of changing surface ocean conditions on the dissolution of aerosol iron, *Global Biogeochem.*
606 *Cycles*, 28, 1235–1250, <https://doi.org/10.1002/2014GB004921>, 2014.

607 Fitzsimmons, J. N., John, S. G., Marsay, C. M., Hoffman, C. L., Nicholas, S. L., Toner, B. M., German, C.
608 R., and Sherrell, R. M.: Iron persistence in the distal hydrothermal plume supported by dissolved – particulate
609 exchange, *Nat. Geosci.*, 10, 1–8, <https://doi.org/10.1038/ngeo2900>, 2017.

610 Gu, H., Sun, Q., Luo, J., Zhang, J., and Sun, L.: A First Study of the Virulence Potential of a *Bacillus subtilis*
611 Isolate From Deep-Sea Hydrothermal Vent, *Front. Cell. Infect. Microbiol.*, 9, 1–14,
612 <https://doi.org/10.3389/fcimb.2019.00183>, 2019.

613 Hawkes, J. A., Gledhill, M., Connelly, D. P., and Achterberg, E. P.: Characterisation of iron binding ligands
614 in seawater by reverse titration, *Anal. Chim. Acta*, 766, 53–60, <https://doi.org/10.1016/j.aca.2012.12.048>,
615 2013a.

616 Hawkes, J. A., Connelly, D. P., Gledhill, M., and Achterberg, E. P.: The stabilisation and transportation of
617 dissolved iron from high temperature hydrothermal vent systems, *Earth Planet. Sci. Lett.*, 375, 280–290,
618 <https://doi.org/10.1016/j.epsl.2013.05.047>, 2013b.

- 619 Hider, R. C. and Kong, X.: Chemistry and biology of siderophores, *Nat. Prod. Rep.*, 27, 637–657,
620 <https://doi.org/10.1039/b906679a>, 2010.
- 621 Hoffman, C. L., Nicholas, S. L., Ohnemus, D. C., Fitzsimmons, J. N., Sherrell, R. M., German, C. R., Heller,
622 M. I., Lee, J. mi, Lam, P. J., and Toner, B. M.: Near-field iron and carbon chemistry of non-buoyant
623 hydrothermal plume particles, Southern East Pacific Rise 15°S, *Mar. Chem.*, 201, 183–197,
624 <https://doi.org/10.1016/j.marchem.2018.01.011>, 2018.
- 625 Hoffman, C. L., Schladweiler, C., Seaton, N. C. A., Nicholas, S. L., Fitzsimmons, J., Sherrell, R. M., German,
626 C. R., Lam, P., and Toner, B. M.: Diagnostic morphology and solid-state chemical speciation of
627 hydrothermally derived particulate Fe in a long-range dispersing plume, *ACS Earth Sp. Chem.*, 4, 1831–
628 1842, <https://doi.org/10.1021/acsearthspacechem.0c00067>, 2020.
- 629 Homann, V. V., Sandy, M., Tincu, J. A., Templeton, A. S., Tebo, B. M., and Butler, A.: Loihichelins A - F ,
630 a Suite of Amphiphilic Siderophores Produced by the Marine Bacterium Halomonas LOB-5, *J. Nat. Prod.*,
631 72, 884–888, 2009.
- 632 Kato, C. and Nogi, Y.: Correlation between phylogenetic structure and function : examples from deep-sea
633 *Shewanella*, 35, 223–230, 2001.
- 634 Kelley, D. S. and Shank, T. M.: Hydrothermal systems: A decade of discovery in slow spreading
635 environments, *Geophys. Monogr. Ser.*, 188, 369–407, <https://doi.org/10.1029/2010GM000945>, 2010.
- 636 Kulmer, W. and Ingalls, A. E.: The R Journal: Tidy Data Neatly Resolves Mass-Spectrometry’s Ragged
637 Arrays, *R J.*, 2022.
- 638 Lauderdale, J. M., Braakman, R., Forget, G., Dutkiewicz, S., and Follows, M. J.: Microbial feedbacks
639 optimize ocean iron availability, *Proc. Natl. Acad. Sci. U. S. A.*, 117, 4842–4849,
640 <https://doi.org/10.1073/pnas.1917277117>, 2020.
- 641 Li, M., Toner, B. M., Baker, B. J., Breier, J. a, Sheik, C. S., and Dick, G. J.: Microbial iron uptake as a
642 mechanism for dispersing iron from deep-sea hydrothermal vents., *Nat. Commun.*, 5, 3192,
643 <https://doi.org/10.1038/ncomms4192>, 2014.
- 644 Lough, A. J. M., Tagliabue, A., Demasy, C., Resing, J. A., Mellett, T., Wyatt, N. J., and Lohan, M. C.: The
645 impact of hydrothermal vent geochemistry on the addition of iron to the deep ocean, *Biogeosciences Discuss.*,
646 [preprint], 1–23, <https://doi.org/10.5194/bg-2022-73>, 2022.
- 647 Manck, L. E., Park, J., Tully, B. J., Poire, A. M., Bundy, R. M., Dupont, C. L., and Barbeau, K. A.:
648 Petrobactin, a siderophore produced by *Alteromonas*, mediates community iron acquisition in the global
649 ocean, *ISME J.*, 16, 358–369, <https://doi.org/10.1038/s41396-021-01065-y>, 2022.
- 650 Martinez, J. S., Carter-Franklin, J. N., Mann, E. L., Martin, J. D., Haygood, M. G., and Butler, A.: Structure
651 and membrane affinity of a suite of amphiphilic siderophores produced by a marine bacterium, *Proc. Natl.*
652 *Acad. Sci. U. S. A.*, 100, 3754–3759, <https://doi.org/10.1073/pnas.0637444100>, 2003.
- 653 Mellett, T., Albers, J. B., Santoro, A., Wang, W., Salaun, P., Resing, J., Lough, A. J. ., Tagliabue, A., Lohan,
654 M., Bundy, R. M., and Buck, K. N.: Particle exchange mediated by organic ligands in incubation experiments
655 of hydrothermal vent plumes along the mid-Atlantic Ridge, n.d.
- 656 Moore, L. E., Heller, M. I., Barbeau, K. A., Moffett, J. W., and Bundy, R. M.: Organic complexation of iron
657 by strong ligands and siderophores in the eastern tropical North Pacific oxygen deficient zone, *Mar. Chem.*,
658 236, 104021, <https://doi.org/10.1016/j.marchem.2021.104021>, 2021.
- 659 Omanović, D., Garnier, C., and Pižeta, I.: ProMCC: An all-in-one tool for trace metal complexation studies,
660 *Mar. Chem.*, 173, 25–39, <https://doi.org/10.1016/j.marchem.2014.10.011>, 2015.
- 661 Parada, A. E., Needham, D. M., and Fuhrman, J. A.: Every base matters: Assessing small subunit rRNA

662 primers for marine microbiomes with mock communities, time series and global field samples, *Environ.*
663 *Microbiol.*, 18, 1403–1414, <https://doi.org/10.1111/1462-2920.13023>, 2016.

664 Park, J., Durham, B. P., Key, R. S., Groussman, R. D., Pinedo-Gonzalez, P., Hawco, N. J., John, S. G.,
665 Carlson, M. C. G., Lindell, D., Juranek, L., Ferrón, S., Ribalet, F., Armbrust, E. V., Ingalls, A. E., and Bundy,
666 R. M.: Siderophore production and utilization by microbes in the North Pacific Ocean, *bioRxiv*,
667 2022.02.26.482025, <https://doi.org/10.1101/2022.02.26.482025>, 2022.

668 Park, J., Durham, B. P., Key, R. S., Groussman, R. D., Pinedo-Gonzalez, P., Hawco, N. J., John, S. G.,
669 Carlson, M. C. G., Lindell, D., Juranek, L., Ferrón, S., Ribalet, F., Armbrust, E. V., Ingalls, A. E., and Bundy,
670 R. M.: Siderophore production and utilization by microbes in the North Pacific Ocean, *Limnol. Oceanogr.*,
671 2022.02.26.482025, <https://doi.org/10.1002/lno.12373>, 2023.

672 Quast, C., Pruesse, E., Yilmaz, P., Gerken, J., Schweer, T., Yarza, P., Peplies, J., and Glöckner, F. O.: The
673 SILVA ribosomal RNA gene database project: Improved data processing and web-based tools, *Nucleic Acids*
674 *Res.*, 41, 590–596, <https://doi.org/10.1093/nar/gks1219>, 2013.

675 Resing, J. a., Sedwick, P. N., German, C. R., Jenkins, W. J., Moffett, J. W., Sohst, B. M., and Tagliabue, A.:
676 Basin-scale transport of hydrothermal dissolved metals across the South Pacific Ocean, *Nature*, 523, 200–
677 203, <https://doi.org/10.1038/nature14577>, 2015.

678 Ruttkies, C., Schymanski, E. L., Wolf, S., Hollender, J., and Neumann, S.: MetFrag relaunched: incorporating
679 strategies beyond in silico fragmentation, *J. Cheminform.*, 8, 1–16, [https://doi.org/10.1186/s13321-016-](https://doi.org/10.1186/s13321-016-0115-9)
680 0115-9, 2016.

681 Sander, S. G. and Koschinsky, A.: Metal flux from hydrothermal vents increased by organic complexation,
682 *Nat. Geosci.*, 4, 145–150, <https://doi.org/10.1038/ngeo1088>, 2011.

683 Sandy, M. and Butler, A.: Microbial iron acquisition: marine and terrestrial siderophores., *Chem. Rev.*, 109,
684 4580–95, <https://doi.org/10.1021/cr9002787>, 2009.

685 Santoro, A. E., Casciotti, K. L., and Francis, C. A.: Activity, abundance and diversity of nitrifying archaea
686 and bacteria in the central California Current, *Environ. Microbiol.*, 12, 1989–2006,
687 <https://doi.org/10.1111/j.1462-2920.2010.02205.x>, 2010.

688 Sorokina, M., Merseburger, P., Rajan, K., Yirik, M. A., and Steinbeck, C.: COCONUT online: Collection of
689 Open Natural Products database, *J. Cheminform.*, 13, 1–13, <https://doi.org/10.1186/s13321-020-00478-9>,
690 2021.

691 Stephens, B. M., Opalk, K., Petras, D., Liu, S., Comstock, J., Aluwihare, L. I., Hansell, D. A., and Carlson,
692 C. A.: Organic Matter Composition at Ocean Station Papa Affects Its Bioavailability, Bacterioplankton
693 Growth Efficiency and the Responding Taxa, *Front. Mar. Sci.*, 7, <https://doi.org/10.3389/fmars.2020.590273>,
694 2020.

695 Sumner, L. W., Amberg, A., Barrett, D., Beale, M. H., Beger, R., Daykin, C. A., Fan, T. W.-M., Fiehn, O.,
696 Goodacre, R., Griffin, J. L., Hankemeier, T., Hardy, N., Harnly, J., Higashi, R., Kopka, J., Lane, A. N.,
697 Lindon, J. C., Marriott, P., Nicholls, A. W., Reily, M. D., Thaden, J. J., and Viant, M. R.: Proposed minimum
698 reporting standards for chemical analysis, *Metabolomics*, 3, 211–221, [https://doi.org/10.1007/s11306-007-](https://doi.org/10.1007/s11306-007-0082-2)
699 0082-2, 2007.

700 Tagliabue, A., Bowie, A. R., Boyd, P. W., Buck, K. N., Johnson, K. S., and Saito, M. A.: The integral role
701 of iron in ocean biogeochemistry, *Nature*, 543, 51–59, <https://doi.org/10.1038/nature21058>, 2017.

702 Toner, B. M., Fakra, S. C., Manganini, S. J., Santelli, C. M., Marcus, M. a., Moffett, J. W., Rouxel, O.,
703 German, C. R., and Edwards, K. J.: Preservation of iron(II) by carbon-rich matrices in a hydrothermal plume,
704 *Nat. Geosci.*, 2, 197–201, <https://doi.org/10.1038/ngeo433>, 2009.

705 Tortell, P. D., Maldonado, M. T., and Price, N. M.: The role of heterotrophic bacteria in iron-limited ocean

706 ecosystems, *Nature*, 383, 330–332, <https://doi.org/10.1038/383330a0>, 1996.

707 Vraspir, J. M. and Butler, A.: Chemistry of marine ligands and siderophores., *Ann. Rev. Mar. Sci.*, 1, 43–63,
708 <https://doi.org/10.1146/annurev.marine.010908.163712>, 2009.

709 Waska, H., Koschinsky, A., Ruiz Chanco, M. J., and Dittmar, T.: Investigating the potential of solid-phase
710 extraction and Fourier-transform ion cyclotron resonance mass spectrometry (FT-ICR-MS) for the isolation
711 and identification of dissolved metal-organic complexes from natural waters, *Mar. Chem.*, 173, 78–92,
712 <https://doi.org/10.1016/j.marchem.2014.10.001>, 2015.

713

714

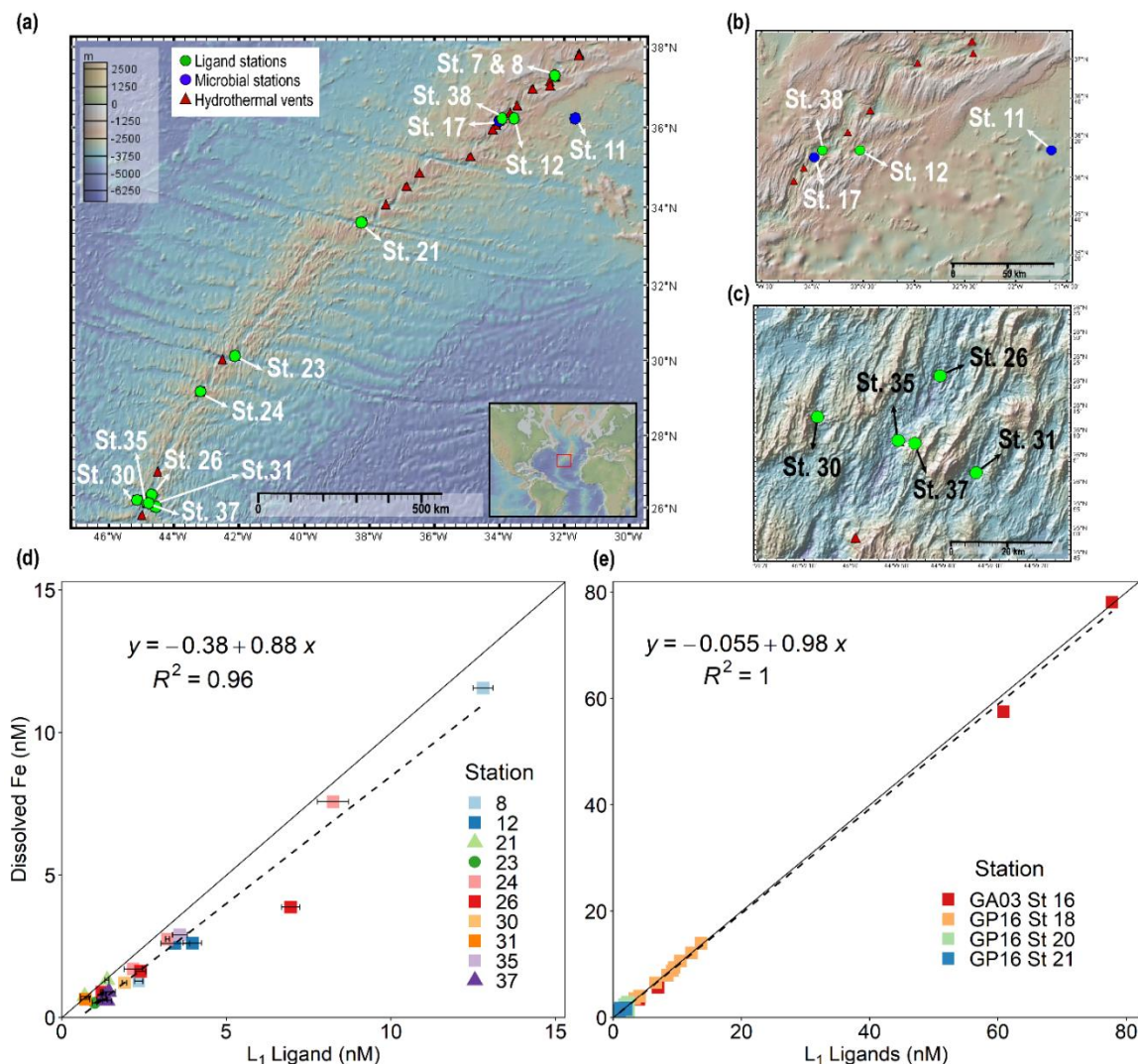
715

716

717

718

719



722

723 **Figure 1. Dissolved iron is strongly correlated with L₁ iron-binding ligands in diverse hydrothermal**724 **systems.** (a) Station map showing the 11 sites investigated along the MAR. Known hydrothermal vents are

725 marked as red triangles(Beaulieu and Szafranski, 2020). Two expanded inset maps for (b) Rainbow and (c)

726 TAG hydrothermal vent fields. For additional information about vent site characteristics refer to **Table 1**. (d)727 dFe versus L₁ iron-binding ligands at each vent site in this study showing a ~1:1 correlation ($m = 0.88$, $R^2 =$ 728 0.96) with dFe in neutrally-buoyant plumes along the MAR. (e) dFe versus L₁ ligands from previous studies

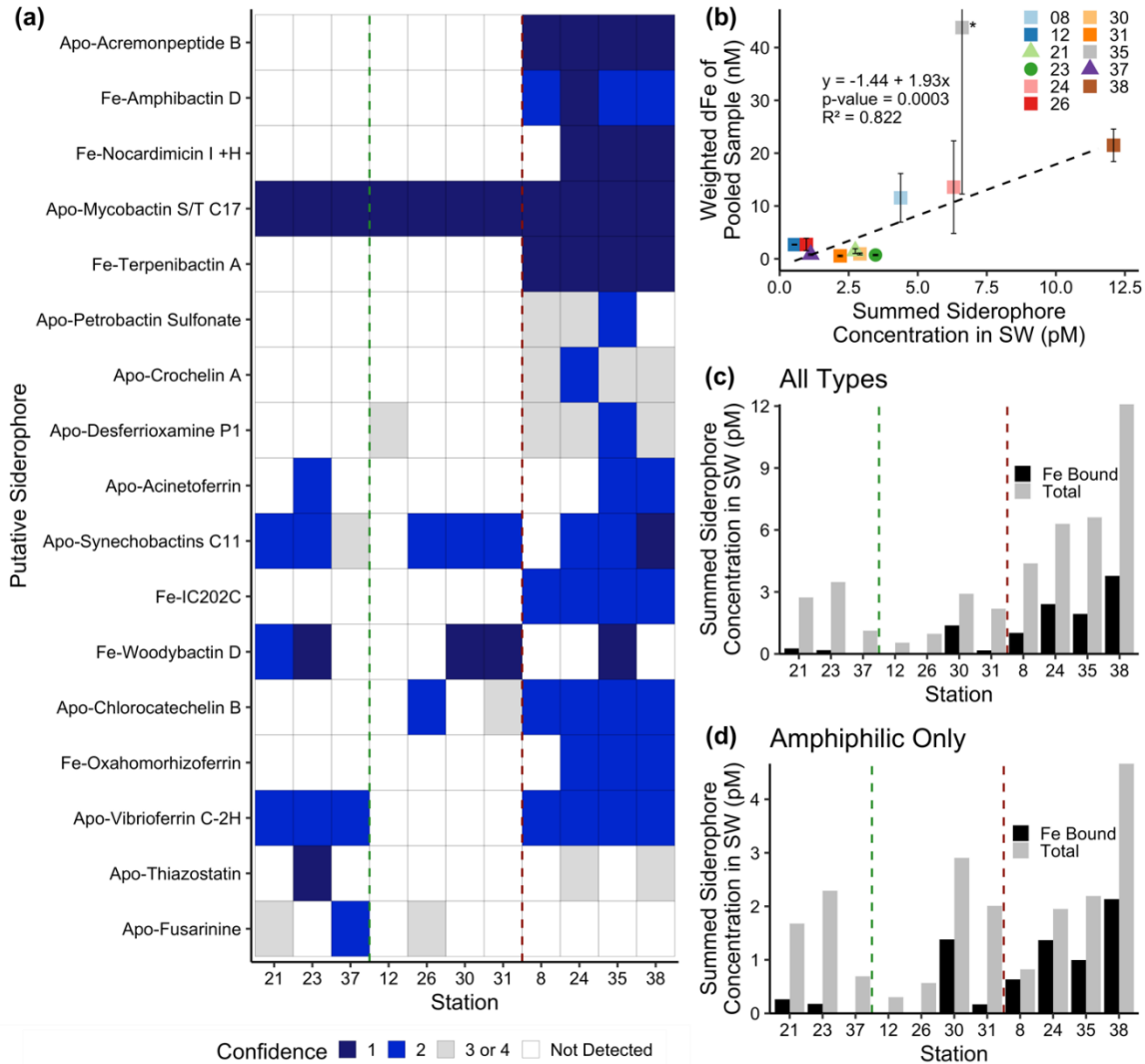
729 over the ridge axis and ~80 km from ridge axis in the Southern East Pacific Rise hydrothermal plume(Buck

730 et al., 2018), and over TAG hydrothermal vent field(Buck et al., 2015). The solid black lines in (d) and (e)

731 are the 1:1 ratio line between dFe and ligand concentrations, and dashed lines show the linear regression for

732 the corresponding data. Square symbols refer to spreading centers, triangles refer to fracture zones, and

733 circles refer to alkaline vents. Error bars represent the 95% confidence interval of the data fit as calculated
734 by ProMCC(Omanović et al., 2015). The map was created using GeoMapApp version 3.6.14.
735
736

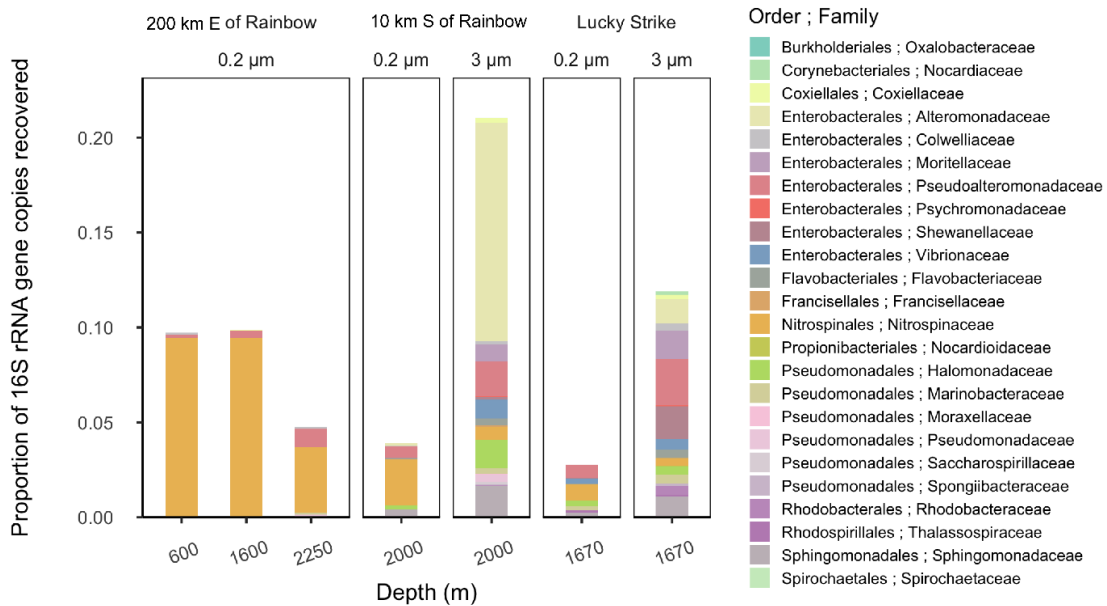


737

738

739 **Figure 2. Siderophore presence in hydrothermal plumes along the MAR.** (a) Heat map of confidence
 740 levels 1-2 (blue gradient, 1 = highest confidence). Gray boxes indicate a detection with lower confidence (see
 741 Methods), and white boxes indicate no detection at those sites. The y-axis is ordered from top to bottom in
 742 terms of descending mass of the apo (without Fe) form of the siderophore. (b) Model II ordinary least squares
 743 regression on dFe versus summed siderophore concentrations (of detections in Fig. 2b), calculated from peak
 744 areas, at each site. Since the siderophore analysis was performed on pooled samples, the dFe values in the
 745 regression are weighted values based on measured dFe and volume of each constituent of the pooled sample.
 746 The vertical error bars represent the standard deviation of dFe of the constituents. TAG (St. 35) — denoted
 747 by the asterisk — was TAG (St. 35) was not included in the regression due to its large range of dFe values
 748 and outlier behavior. (c-d) Fe bound versus total summed concentration of (c) all types of siderophores and
 749 (d) amphiphilic siderophores at each station. The vertical green lines separate fracture/diffuse sites from off-
 750 axis sites and vertical red lines separate off-axis from on-axis sites as defined in Table 1. Symbols follow
 751 Fig. 1.

752



753

754

755 **Figure 3. Relative abundance of putative siderophore-producing taxa.** Bar height indicates the proportion
 756 of 16S rRNA genes recovered in each sample, separated by depth from water surface, filter size fraction, and
 757 site location. Colors correspond to taxonomy. Genera found in MAR vent microbial communities with
 758 members in the antimash database predicted to produce siderophores are depicted at the family level.

759

Table 1. Characteristics of sample locations along the Mid Atlantic Ridge.

Vent Names	Abbr.	Station	Geology	Host rock	Vent type	Spreading rate (mm/yr)	Summed putative siderophore concentration (pM)	Summed Siderophore concentration/ L ₁ ligand (%)*
Lucky Strike	LS	7/8	Spreading Center	gabbro	Black smoker	20.2	4.38	0.034-0.19
33 km E of Rainbow	CER	12	Spreading Center	-	-	-	0.537	0.013-0.017
Rainbow	R	38	Spreading Center	ultramafic	Black smoker	20.6	12.1	<i>n.a.</i>
Hayes Fracture Zone	HFZ	21	Fracture Zone	peridotites/gabbro	-	21.2	2.74	0.20-0.39
Lost City	LC	23	Fracture Zone	ultramafic/gabbro	Alkaline	22.6	3.47	0.27-0.35
Broken Spur	BS	24	Spreading Center	gabbro	Black smoker/diffuse	22.9	6.30	0.07-0.29
29 km N of TAG	CNT	26	Spreading Center	-	-	-	0.968	0.014-0.079
30 km W of TAG	CWT	30	Spreading Center	-	-	-	2.91	0.15
30 km E of TAG	CET	31	Spreading Center	-	-	-	2.19	0.31

Trans-Atlantic Geotraverse	TAG	35	Spreading Center	gabbro	Black smoker	23.6	6.61	0.18
Low Temp Slope	LTS	37	-	-	Diffuse fluids	-	1.13	0.079-0.087

Spreading rates along the Mid-Atlantic Ridge were gathered from the Interridge Database v3.4. Host rock groups were determined from previously discussed classifications (Bazylev, 1997; Kelley and Shank, 2010). Off-axis sites –33 km E of Rainbow, 29 km N of TAG, 30 km E of TAG, and 30 km W of TAG– were far-field locations of their respective vent field. Low Temp Slope was a diffuse-dominated site that was sampled for the first time as a part of this study. Summed putative siderophore concentrations and the percent of L₁ ligand are reported for compounds detected with at least confidence level 1 and 2 at one site. These values do not take into account typical extraction efficiencies of ENV columns for Fe-binding organics. Average L₁ ligand and siderophore concentrations can be viewed in **Table S3** and concentrations for individual siderophores can be observed in **Table S5**.

*The siderophore sample at each site was pooled from ligand samples, so the percentage of siderophores in the L₁ pool is presented as a range based on the range of L₁ concentrations at each site.

n.a. = unable to be determined

- = unknown

